Self-consistent quantum Monte Carlo simulations of the structure of the liquid-vapor interface of a eutectic indium-gallium alloy

Stuart A. Rice and Meishan Zhao
Department of Chemistry and The James Franck Institute, The University of Chicago, Chicago, Illinois 60637
(Received 20 November 1997; revised manuscript received 6 February 1998)

We report the results of self-consistent quantum Monte Carlo simulations of the density distribution along the normal to the liquid-vapor interface, and the in-plane structure function, of the liquid-vapor interface of a eutectic binary alloy of indium and gallium (16.5% In) at 86 °C. The density distribution along the normal to the interface exhibits layering, with a sensibly complete monolayer of In outermost in the interface. Our results are in good agreement with the experimental data of Regan *et al.* [Phys. Rev. B **55**, 15874 (1997)]. We also report the results of self-consistent quantum Monte Carlo simulations of the structure of the liquid-vapor interfaces of In:Ga alloys with In concentrations greater than and less than the eutectic concentration. The In atoms segregate in the outermost layer of the interface as a sensibly complete monolayer when the bulk In concentration is 25% and as a partial monolayer when the bulk In concentration is 11%. In these cases, as well as for the eutectic alloy, there is some Ga well mixed with the In in the outermost layer of the stratified liquid-vapor interface. And for all alloy compositions studied the layer of the interface beneath the monolayer of segregated In is deficient in In relative to the bulk concentration; the bulk concentration of In is reached in the third layer of the liquid-vapor interface.
[S0163-1829(98)03521-8]

I. INTRODUCTION

Although there has been considerable progress in understanding the properties of the liquid-metal–vapor interface,[1–29] much remains to be discovered. It is now well established that the liquid-metal–vapor interface is different from the simple nonmetallic liquid-vapor interface because of the variation of the local electronic structure with electron density in the interface region, which leads to a strong variation of the effective ion-ion interactions and the binding energy per ion with position in the interface. The results of self-consistent Monte Carlo simulation studies[1–17] of the liquid-vapor interface of a pure metal, in which the electron-ion interaction is described in the pseudopotential representation and the electron density distribution that defines the nonlocal pseudopotential is determined from solution of the Kohn-Sham equation,[30,31] show that the longitudinal ion distribution is stratified over a region extending several atomic diameters into the bulk. The simulation results also show, unexpectedly, that the transverse (in-plane) pair correlation function in the interface is essentially the same as the pair correlation function in the bulk liquid, a result which implies that the strict local density approximation to a system with inhomogeneous spatial density distribution, whether pure or a mixture, must be replaced by a nonlocal representation that includes to first order the force responsible for maintaining the nontrivial longitudinal density distribution. The predicted stratification of the liquid-vapor interface of a pure metal has been strikingly confirmed by Regan *et al.*, via x-ray-reflectivity studies, for Ga (Refs. 19–22) and Hg (Ref. 18). The predicted similarity between the transverse structure function in the liquid-vapor interface and the structure function in the bulk liquid metal has been confirmed by Rice and co-workers, via grazing-incidence x-ray-diffraction measurements, for Hg (Ref. 24) and Ga (Refs. 25 and 27).

Since differences in atomic size and valence between the components of an alloy will lead to differences in the local electron density about each ion core, we must expect that the longitudinal distributions of the components in the liquid-vapor interface of an alloy will have a composition substructure which reflects the influence of the interactions in the interface. Calculations reported by Gryko and Rice[11–13] and by Harris, Gryko, and Rice[9] show that in the liquid-vapor interface of a mixture of Cs and Na there are three important structural features: (i) The overall (all species) longitudinal density distribution is stratified for three to four atomic diameters into the bulk liquid, (ii) the segregation of Cs in the interface takes the form of a monolayer of essentially pure Cs in the outermost region of the liquid-vapor transition region, and (iii) in addition to (i) and (ii) there is other weak structure associated with the longitudinal distribution of the excess Cs in the interface; namely, the atomic layer beneath the monolayer of Cs is deficient in Cs relative to the bulk concentration. The bulk concentration is reached in the third-to-fourth atomic layer. Because of the limited range of the electron densities associated with homovalent metals, we expect these structural features to be generic to the class of homovalent alloys irrespective of the valence. Indeed, the results of grazing-incidence x-ray-diffraction and x-ray-reflectivity studies of the liquid-vapor interface of a dilute alloy of Bi in Ga (0.2% Bi) (Refs. 25 and 27) reveal that the excess Bi concentration in the interface is concentrated in a monolayer, that the Bi monolayer has the structure of a supercooled liquid, and that the stratification of the longitudinal density distribution of the Ga host is sensibly the same as in pure Ga, all in agreement with structural features (i) and (ii) cited above. Zhao, Chekmarev, and Rice[17] have shown that the results of self-consistent quantum Monte Carlo simulations of the liquid-vapor interface of this alloy are in good

agreement with the experimentally determined transverse structure function and longitudinal density distribution. Moreover, an important qualitative characteristic of the liquid-vapor interface of this dilute Bi:Ga alloy, namely, that the excess Bi atoms are atop the Ga in a separate layer, and not mixed with Ga, is correctly reproduced by the theoretical calculations. The third of the above-cited structural features inferred from the simulations of the liquid-vapor interface of Cs:Na alloys cannot be tested in the very dilute Bi:Ga alloy.

Regan and co-workers have reported[23] x-ray-reflectivity studies of a eutectic alloy of In with Ga (16.5% In); they conclude that the excess In concentration in the interface is concentrated in a monolayer. In this paper we report the results of self-consistent quantum Monte Carlo simulations of the structure of the liquid-vapor interface of the eutectic In:Ga alloy studied by Regan *et al.* The In:Ga binary alloy system differs from the Bi:Ga binary alloy system in that In is very soluble in liquid Ga, whereas Bi has only a very small solubility in Ga near its melting point. The longitudinal density profile obtained from the simulations of the liquid-vapor interface of the eutectic In:Ga alloy is in good agreement with that deduced from the experimental data.

We also report the results of self-consistent quantum Monte Carlo simulations of the structure of the liquid-vapor interfaces of In:Ga alloys with In concentrations greater than and less than the eutectic concentration. Unlike the Bi:Ga system, it is found that for all values of the excess interface concentration of In we have studied there is also some Ga in the outermost layer of the liquid-vapor interface and that the In and Ga atoms are well mixed in the outermost layer of the interface. Moreover, it is found that the layer of the interface beneath the monolayer of segregated In is deficient in In relative to the bulk concentration; the bulk concentration of In is reached in the third layer of the liquid-vapor interface, just as has been previously predicted for the case of Cs in liquid-vapor interfaces of Cs:Na alloys.[1,9,13]

II. CALCULATIONS

A detailed description of the self-consistent quantum Monte Carlo method we use has been published elsewhere, and so in this section we provide only a sketch of the theoretical analysis. Our analysis is based on a density-functional self-consistent pseudopotential representation with the system Hamiltonian

$$H=\sum_{i=1}^{N}\left[\frac{\mathbf{p}_i^2}{2m_i}+\sum_{j<i}\phi_{\mathrm{eff}}(\mathbf{R}_{ij};n_e(\mathbf{r}))\right]+U_0(\rho(\mathbf{r}),n_e(\mathbf{r})) \tag{2.1}$$

and a quantum Monte Carlo simulation procedure developed by Rice and co-workers. In Eq. (2.1), $U_0(\rho(\mathbf{r}),n_e(\mathbf{r}))$ is the so-called structure-independent potential energy as a function of the electronic density, $n_e(\mathbf{r})$, and the ionic density, $\rho(\mathbf{r})$, $\mathbf{r}$ and $\mathbf{R}$ are the coordinates of an electron and an ion, respectively, $\mathbf{p}_i$ and m_i are the ith ion momentum and mass, and $\phi_{\mathrm{eff}}(\mathbf{R}_{ij};n_e(\mathbf{r}))$ is the effective ion pair potential.

The system Hamiltonians for binary alloys and pure metals are very similar, the only difference being that the pair potential energy and the one-body potential energy in the alloy depend on both the types and the positions of ions. The structure independent energy $U_0(\rho(\mathbf{r}),n_e(\mathbf{r}))$ is represented as a density functional with the local density approximation,

$$\begin{aligned}U_0(\rho_0(\mathbf{r}),n_e(\mathbf{r}))=&\frac{3(3\pi^2)^{2/3}\sigma}{10}\int_0^\infty dz[n_e(\mathbf{r})]^{5/3}+\frac{\sigma}{72}\int_0^\infty dz\,\frac{|\nabla^2 n_e(\mathbf{r})|}{n_e(\mathbf{r})}+\frac{\sigma}{540(3\pi^2)^{2/3}}\int_0^\infty dz\Bigg\{[n_e(\mathbf{r})]^{1/3}\Bigg[\left(\frac{\nabla^2 n_e(\mathbf{r})}{n_e(\mathbf{r})}\right)^2\\&-\frac{9}{8}\left(\frac{\nabla^2 n_e(\mathbf{r})}{n_e(\mathbf{r})}\right)\left(\frac{\nabla n_e(\mathbf{r})}{n_e(\mathbf{r})}\right)^2+\frac{1}{3}\left(\frac{\nabla n_e(\mathbf{r})}{n_e(\mathbf{r})}\right)^4\Bigg]\Bigg\}^2-2\pi\sigma\int_0^\infty dz\int_0^\infty dz'[\rho_0(z)\rho_0(z')-n_e(z)n_e(z')]|z'-z|\\&+2\sigma\int_0^\infty n_e(z)\varepsilon_{xc}(n_e(z))dz+2\sigma\int_0^\infty dz\,\rho_0(z)\varepsilon_{ps}(n_e(z)),\end{aligned} \tag{2.2}$$

where σ is the area of the liquid-vapor interface. The terms in Eq. (2.2) are, in sequence, the electronic kinetic energies, the electrostatic energy of the system arising from the difference between the electron and ion density distributions in the liquid-vapor interface transition zone, the exchange-correlation contribution to the energy using the homogeneous electron gas as proposed by Vosko *et al.*[32] and by Langreth and Mehl,[33] and the electron-ion pseudopotential contribution to the electronic energy with $\varepsilon_{ps}(n_e(z))$ the ionic pseudopotential a function of the valence electron density distribution.

For a binary alloy the pseudopotential contribution to the structure-independent energy is given by

$$\begin{aligned}\varepsilon_{ps}=&\frac{3}{k_F^3}\int_0^{k_F}f(q,q')q^2dq-\frac{1}{\pi}\sum_{i=1}^{2}X_i\\&\times\int_0^\infty dq[\overline{Z_i^2}|M_i(q)|^2-(z_i^*)^2F_{ii}(q)]-\frac{2\pi}{\Omega}\\&\times\sum_{i=1}^{2}\sum_{j=1}^{2}z_i^*z_j^*X_iX_j\lim_{q\to0}\frac{1-F_{ij}(q)}{q^2},\end{aligned} \tag{2.3}$$

where k_F is the Fermi wave number, $f(q,q')$ is the nonlocal bare electron-ion pseudopotential matrix, $M(q)$ is the Fourier transform of the depletion hole distribution, X_i is the

mole fraction of the ith component, $\bar{Z}$ is the depletion hole charge, and $F_{ij}(q)$ is the normalized energy wave-number characteristic function. The effective ion pair interaction potential $\phi_{\rm eff}(R_{ij})$ is calculated using the local density approximation

$$\phi_{\rm eff}(R_{ij})=\frac{z_i^* z_j^*}{R_{ij}}\left\{1-\frac{1}{\pi}\int_0^\infty [F_{ij}(q)+F_{ji}(q)] \times \sin(qR_{ij})q^{-1}dq\right\}+\varepsilon(R_{ij}), \tag{2.4}$$

where z_i^* and z_j^* are the effective valences of the ions and $\varepsilon(R_{ij})$ is a small correction to the pair potential including the van der Waals core polarization interaction and the Born-Mayer core-core repulsion.

For a given positive jellium distribution, the electron density can be obtained by solving the Kohn-Sham[30,31] equation,

$$\left[-\frac{\hbar^2}{2m}\frac{d^2}{dz^2}+V_{\rm eff}(z,n_e(z))\right]\psi_n(z)=\varepsilon_n\psi_n(z), \tag{2.5}$$

where $V_{\rm eff}(z)$ is an effective potential energy including the electron-electron interaction, electron-ion interaction, and the exchange-correlation contribution. Because the electron density falls to zero rapidly outside the jellium distribution with the Gibbs dividing surface at $z=z_0$, it is a good approximation to treat the electronic system as bounded in z; this is accomplished by setting $n_e(z)=0$ at a fairly large distance outside the jellium distribution, which, in turn, is accomplished by including in $V_{\rm eff}(z,n_e(z))$ an infinite hard wall potential located at $z_w=\pm(z_0+\delta)$. The parameter δ is chosen large enough so that $n_e(z_w)=0$, and numerical accuracy is retained in the calculations. For the calculations reported in this paper, we set $\delta=15a_0$, where $a_0=0.53$ Å is the Bohr radius. For the simulations reported below, which employ a slab of 2000 ions and 6000 electrons, the Gibbs dividing surface is located at $z_0=51.6a_0$.

The Kohn-Sham equation is solved self-consistently since the eigenvector sought, $\psi_n(z)$, is used in the construction of $V_{\rm eff}(z,n_e(z))$, and the corresponding electron density is obtained from

$$n_e(z)=\sum_n f_n|\psi_n(z)|^2, \tag{2.6}$$

where f_n is the nth state electron occupation number.

The dimensions of the simulation slab were $L_0\times L_0\times 2L_0$ in the x, y, and z directions. The slab contains two free surfaces located at, approximately, $\pm z_0$, each with area $\sigma=(L_0)^2$; periodic boundary conditions were applied in the x and y directions. The length L_0 was chosen such that the average density of ions in the slab matched the density of liquid Ga at the simulation temperature. The center of mass of the simulation system was located at the origin of the coordinates ($x=0$, $y=0$, $z=0$). The initial ion configuration was generated subject to the constraint that there be no ion core overlaps. We take one Monte Carlo simulation pass to be 2000 ionic configurations; our calculations were carried out for 28 000 Monte Carlo passes.

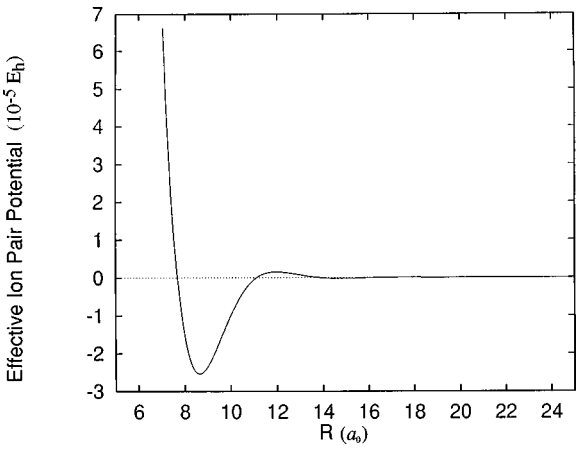

FIG. 1. Concentration-weighted effective ion-ion pair potential in bulk liquid In:Ga (16.5% In) at 86 °C and a density of 0.052 58 atoms/Å^3.

III. RESULTS

Figure 1 displays the effective ion-ion pair potential at a liquid density of 0.05258 atoms/Å^3, calculated using the energy-independent model pseudopotential proposed by Woo, Wang, and Matsuura.[34,35] Figure 2 shows the calculated pair correlation functions of bulk liquid indium, gallium, and the eutectic (16.5%) indium-gallium alloy at 86 °C. One test of the accuracy of our pseudopotential for In is shown in Fig. 3, where the calculated and observed bulk liquid structure[36] functions are compared; the agreement is seen to be excellent.

To correctly mimic the segregation of In in the liquid-vapor interface of an alloy with a bulk concentration of 16.5% In requires that we use a simulation sample which, overall, has about 26% In atoms. This requirement arises because the double-ended simulation sample we have used contains only 2000 atoms. The 2000 ion slab has 18 layers, each with about 111 ion cores, and the Gibbs dividing surfaces are at $z_0=\pm 51.6a_0$. A complete monolayer of In at each liquid-vapor interface requires, in total, about 222 atoms. Assuming that the expected segregation of a full monolayer of In in the liquid-vapor interface occurs, the bulk liq-

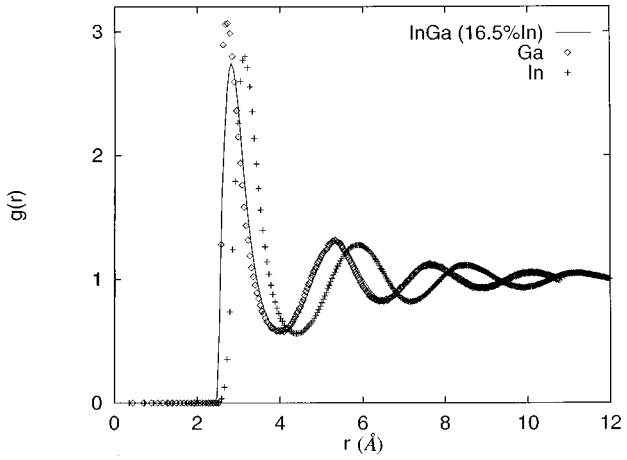

FIG. 2. Pair correlation functions of bulk liquid In:Ga (16.5% In) (diamond), bulk liquid In (dashed line), and bulk liquid Ga (solid line), all at 86 °C.

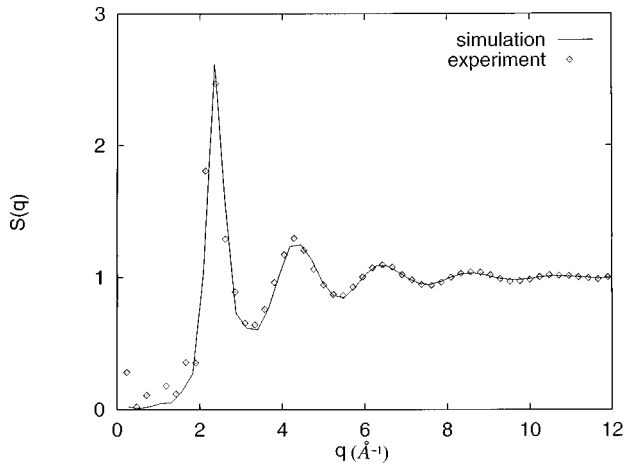

FIG. 3. Comparison of the simulated and observed bulk In structure function at 86 °C.

uid in the simulation slab must then contain about 293 In atoms, and so, overall, the slab should contain 515 In atoms mixed with 1485 Ga atoms. Our simulations were carried out with a slab that has nearly this composition, namely, 520 In atoms and 1480 Ga atoms. We expect the liquid-vapor interface of this model system to accurately mimic that of the macroscopic system because the depth of the bulk liquid in the slab is considerably larger than the range of the pseudopotential and all of the other interactions in the system.

We show, in Fig. 4(a), the overall longitudinal density distribution obtained from simulations using a sample slab with 2000 ions, of which 520 are In. Figures 4(b) and 4(c) display, respectively, the contributions to the longitudinal density distribution from the host Ga and the solute In. These results clearly show the segregation of the excess In in the liquid-vapor interface into a monolayer at the outer edge of the interface. We note that there are a small number of Ga atoms in the outermost layer of the liquid-vapor interface, uniformly mixed with the In atoms.

We have also performed simulations with a slab containing 1000 ions with species ratio In:Ga=0.165:0.835. The resultant density profile is displayed in Fig. 5(a); it was obtained from an average over 37 000 Monte Carlo passes, a number somewhat larger than the 28 000 Monte Carlo passes used to extract information from the simulation of the 2000-ion-slab simulation shown in Fig. 5(b). The results shown in Fig. 5(a) have both a much greater peak amplitude and much greater peak to trough ratio than those shown in Fig. 5(b), a clear indication that the 1000-ion slab is too small to adequately represent the influence of capillary wave excitations. Figure 5(b) displays a comparison of the calculated and observed longitudinal density distributions in the liquid-vapor interface of the eutectic In:Ga alloy. We consider the agreement between calculation and experiment to be very good; the deviations are similar to those found in the previously reported comparisons between the calculated and observed longitudinal density distributions in the liquid-vapor interfaces of pure Ga and a dilute Bi:Ga alloy. These deviations are, we believe, attributable to the inadequate range of capillary wave excitations supported by a 2000-atom slab (relative to the range detected in the experimental studies) and to residual errors in the pseudopotentials used in the simulations.

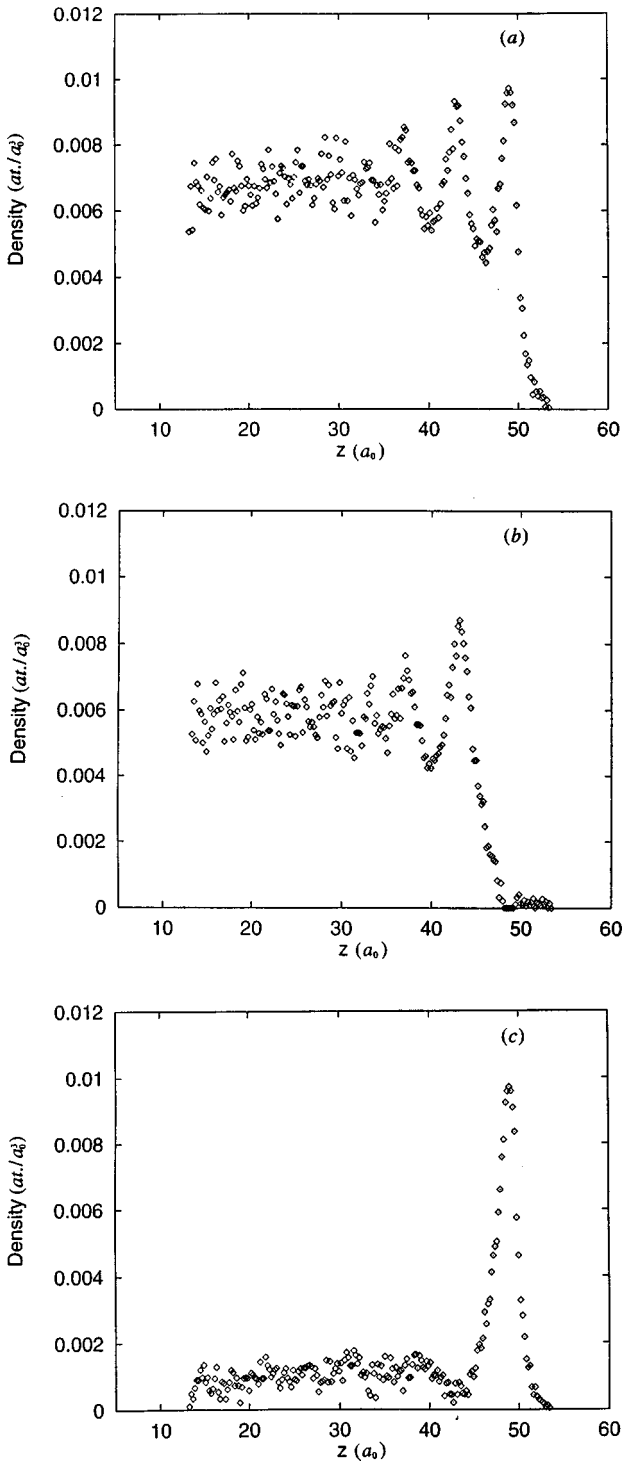

FIG. 4. Longitudinal density profiles in the liquid-vapor interface of In:Ga (16.5% In) at 86 °C: (a) all atoms, (b) Ga, and (c) In.

We have also carried out simulations of the liquid-vapor interface of In:Ga alloys with In concentrations greater than and less than that at the eutectic composition (16.5%). We show in Figs. 6(a) the overall longitudinal density distribution obtained from simulations using a sample slab with 2000 ions, of which 660 are In, which mimics the behavior of a system with a bulk In concentration of 25%. Figures 6(b) and 6(c) display, respectively, the corresponding contributions to the longitudinal density distribution from the host

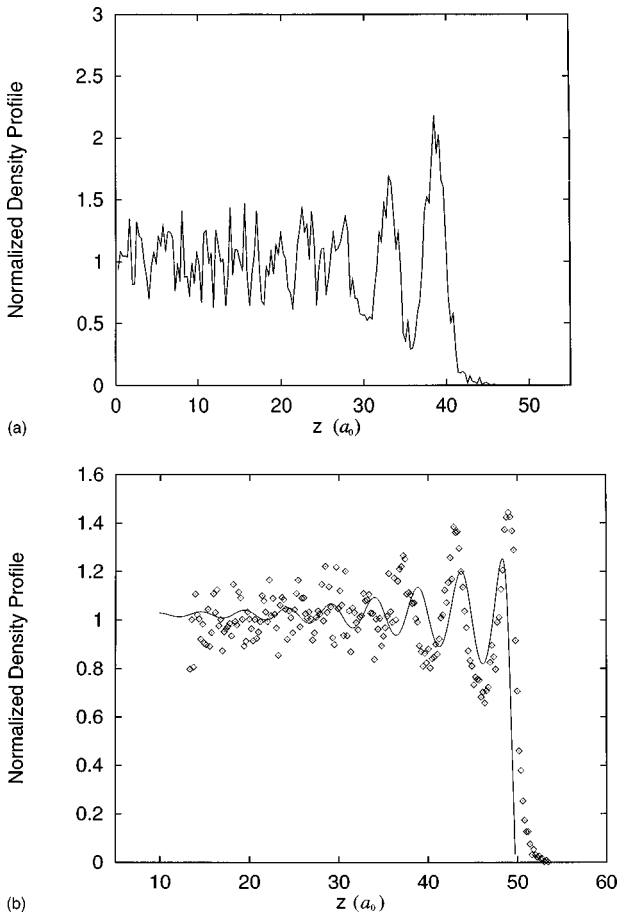

FIG. 5. (a) Longitudinal density distribution in the liquid-vapor interface of In:Ga (16.5% In) at $T=86\,^{\circ}$C from a slab with 1000 ions. (b) Comparison of the calculated (diamond) and experimentally determined (solid line) longitudinal density distributions in the liquid-vapor interface of In:Ga (16.5% In) at $T=86\,^{\circ}$C. This calculated result is from a simulation with a slab of 2000 ions.

Ga and the solute In. The calculations displayed in Fig. 6(b) show that there are more Ga atoms in the outermost layer of the liquid-vapor interface than when the bulk composition is 16%. We also note, from the results displayed in Fig. 6(c), that there is a deficiency in the In concentration in the second layer of the stratified liquid-vapor transition region, just as found in the simulations of the liquid-vapor interface of the Cs:Na system. As in the latter system, the bulk composition of the alloy is established in the third layer of the liquid-vapor interface. Figures 7(a), 7(b), and 7(c) display, respectively, the overall longitudinal density distribution and the corresponding contributions to the longitudinal density distribution from the host Ga and the solute obtained from simulations using a sample slab with 1670 ions, of which 330 are In, corresponding to a bulk phase concentration of about 11% In. The excess concentration of In in the liquid-vapor interface in this system is about one-third that for the eutectic alloy, and the outermost layer of the liquid-vapor transition region is a homogeneous mixture of In and Ga. As in the other In:Ga liquid-vapor interfaces, the second layer is deficient in In and the bulk alloy composition is reached in the third layer.

Finally, we show in Fig. 8 a comparison of the in-plane pair correlation function in the outmoster layer of the liquid-

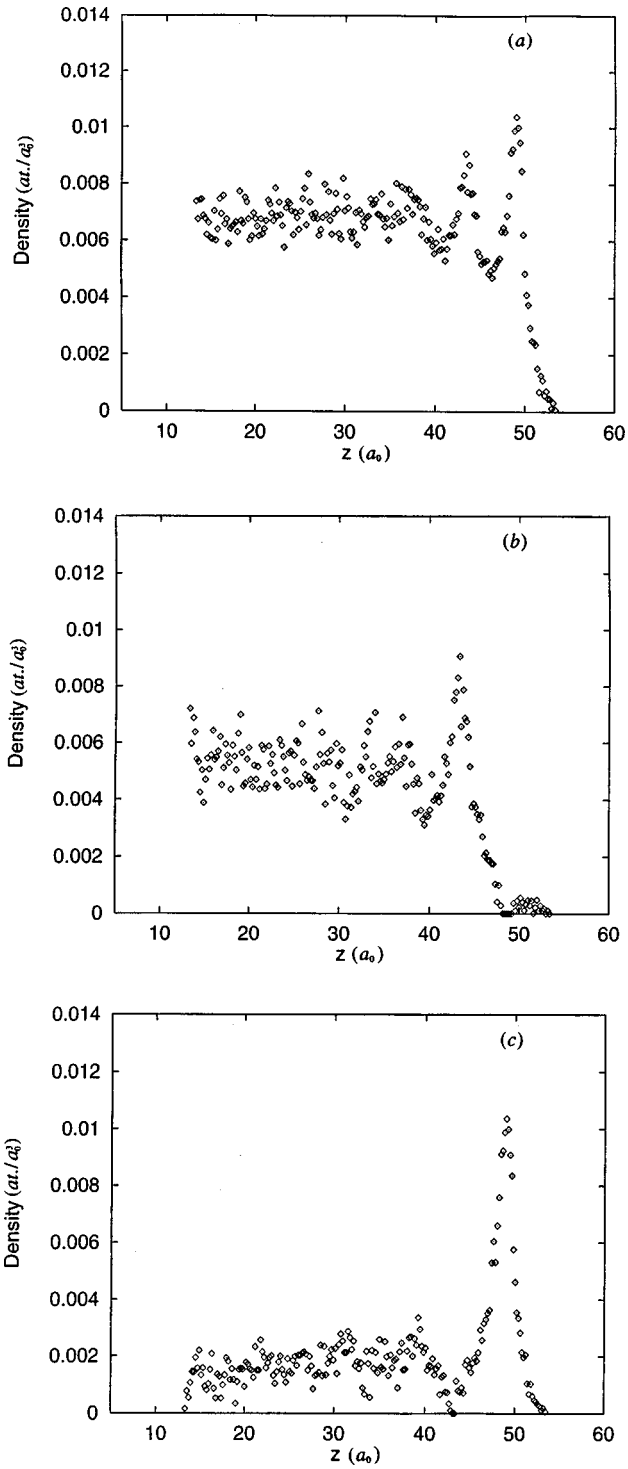

FIG. 6. Logitudinal density profiles in the liquid-vapor interface of In:Ga (25% In) at 86 °C: (a) all atoms, (b) Ga, and (c) In.

vapor interface of the alloy with composition InGa (16.5% In), the calculated bulk liquid In pair correlation function, and the measured bulk liquid In pair correlation function. This figure shows that the transverse pair correlation function in the interface is essentially the same as the pair correlation function in the bulk liquid.

IV. DISCUSSION

The structure of the In:Ga binary alloy liquid-vapor interface obtained from the self-consistent Monte Carlo simula-

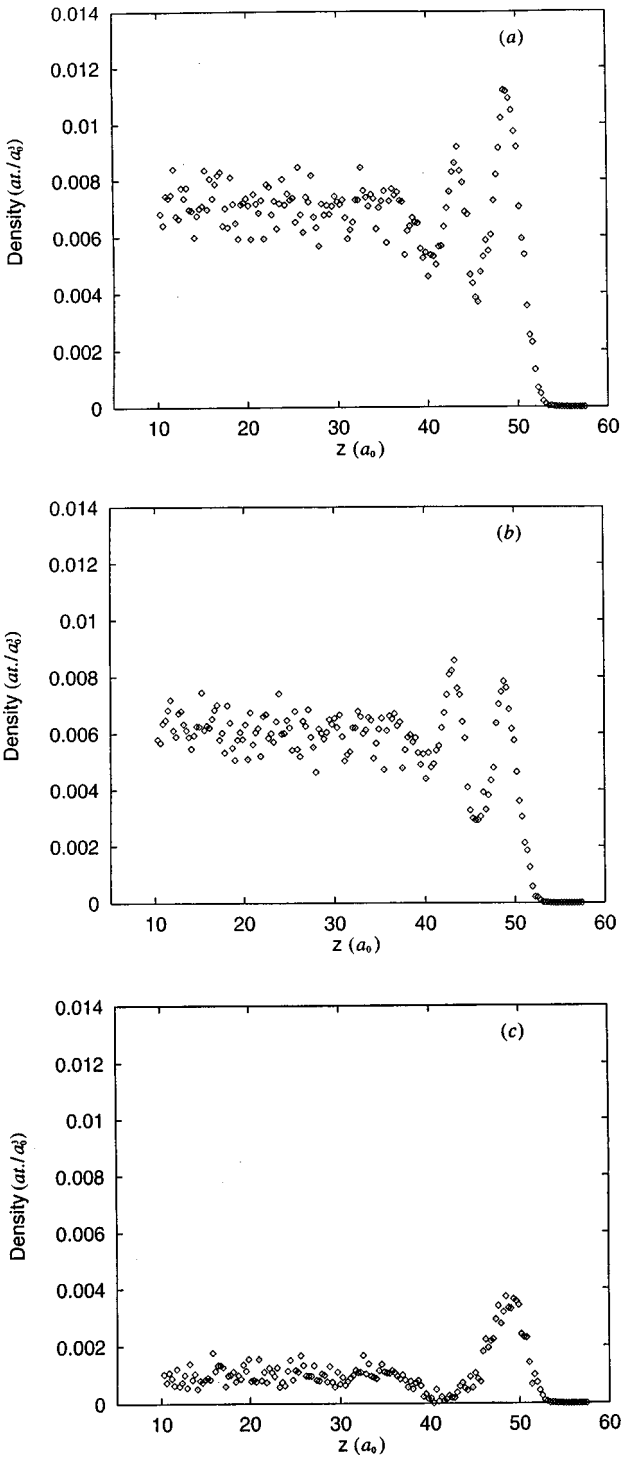

FIG. 7. Logitudinal density profiles in the liquid-vapor interface of In:Ga (11% In) at 86 °C: (a) all atoms, (b) Ga, and (c) In.

tions reported in this paper is in good agreement with that inferred from the x-ray-reflectivity study of this alloy reported by Regan *et al.*[23] Similar good agreement between the calculated and experimentally determined density distributions in the liquid-vapor interfaces of pure Ga and of a dilute Bi:Ga alloy has been reported elsewhere. It should be noted that Regan *et al.* show that their reflectivity data can be fitted with a model in which the segregated In is concentrated in a monolayer atop the bulk liquid alloy and a model in which the concentration of segregated In atoms falls exponentially

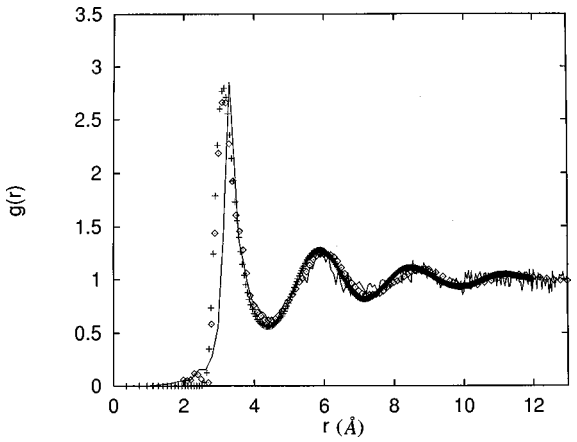

FIG. 8. In-plane pair correlation function in the liquid-vapor interface of the alloy with composition InGa (16.5% In) from simulation (solid line), compared to the calculated bulk In pair correlation function (crosses) and to the measured bulk In pair correlation function (diamonds).

from the fully filled outer layer with a characteristic length of about 1 Å, which corresponds to a second-layer In concentration of 21% (instead of the bulk In concentration of 16.5%). And for the former model of the distribution of In in the interfacial region, they also note that the small difference in In and Ga electron densities permits equally good fits to the reflectivity data with outer layer fillings ranging from 86% to 100%.

We believe the agreement between our simulation results and the experimental data is sufficiently good to take seriously some of the more subtle features of the structure inferred from the simulation results.

The distributions of In in the liquid-vapor interfaces of the three In:Ga alloys we have studied show an absence of In atoms in the second layer. We believe that this structural feature, which is very similar to that found for the Cs atom distribution in self-consistent Monte Carlo simulations of the liquid-vapor interfaces of a number of Cs:Na alloys,[1,9,13] is generic in homovalent liquid binary alloys. Although Regan *et al.* did not consider a model of the In concentration distribution in the liquid-vapor interface that has a minimum in the second layer, we believe that model will fit their reflectivity data as well as those they considered, because of the small difference in the electron densities of In and Ga. In principle, anomalous reflectivity measurements carried to sufficiently large momentum transfer can be used to test the subtler details of the predicted In distribution in the liquid-vapor interface.

From the point of view of thermodynamics, it is irrelevant whether the excess concentration of a component that segregates in the liquid-vapor interface does or does not have a concentration that exceeds the bulk solubility limit. However, this indifference to the bulk solubility limit exhibited by the overall thermodynamics of segregation does not imply that there is a similar indifference with respect to the local structure of the interfacial region, i.e., the longitudinal and transverse spatial distributions of host and segregated components. Comparison of the results of our simulations of the liquid-vapor interfaces of Bi:Ga and In:Ga alloys reveals that in the former case the segregated Bi lies atop the host Ga, forming a completely separated outer layer, while in the lat-

ter case there is miscibility of In and Ga in the outer layer. We suggest that it will generally be the case that when the concentration of the component that segregates in the liquid-vapor interface greatly exceeds the bulk alloy solubility limit, as in the Bi:Ga system, the segregated component will form a separate outer layer which may be partially or fully filled depending on the bulk alloy composition. In such a system there exists the possibility that phase transitions, e.g., two-dimensional gas-to-liquid condensation, can occur in the outer layer of the liquid-vapor interface of the alloy. Also, when the outer layer of the liquid-vapor interface is only partially filled, the effective roughness of the interface is increased relative to that characteristic of the pure host liquid-vapor interface and that characteristic of the alloy with a fully filled outer layer. In contrast, when the components of the bulk liquid alloy have a large range of miscibility, as in the In:Ga system, there is mixing of the segregated and host atoms in the outer layer of the liquid-vapor interface for all bulk liquid compositions, and the roughness of the interface is modified only to the extent that the change in surface tension permits a change in the mean square amplitude of thermal fluctuations.

ACKNOWLEDGMENT

This work has been supported by a grant from the National Science Foundation.

[1] S. A. Rice, Proc. Natl. Acad. Sci. USA **84**, 4709 (1987).
[2] S. A. Rice, J. Gryko, and U. Mohanty, in *Fluid Interfacial Phenomena*, edited by C. A. Croxton (Wiley, New York, 1986).
[3] J. W. Allen and S. A. Rice, J. Chem. Phys. **67**, 5105 (1977); **68**, 5053 (1978).
[4] M. P. D'Evelyn and S. A. Rice, Phys. Rev. Lett. **47**, 1844 (1981).
[5] M. P. D'Evelyn and S. A. Rice, J. Chem. Phys. **78**, 5081 (1983).
[6] M. P. D'Evelyn and S. A. Rice, J. Chem. Phys. **78**, 5225 (1983).
[7] M. P. D'Evelyn and S. A. Rice, Discuss. Faraday Soc. **16**, 71 (1982).
[8] J. G. Harris, J. Gryko, and S. A. Rice, J. Chem. Phys. **87**, 3069 (1987).
[9] J. G. Harris, J. Gryko, and S. A. Rice, J. Stat. Phys. **48**, 1109 (1987).
[10] J. G. Harris and S. A. Rice, J. Chem. Phys. **86**, 7531 (1987).
[11] J. Gryko and S. A. Rice, J. Phys. F **12**, L245 (1982).
[12] J. Gryko and S. A. Rice, J. Non-Cryst. Solids **61-62**, 703 (1984).
[13] J. Gryko and S. A. Rice, J. Chem. Phys. **80**, 6318 (1984).
[14] S. A. Rice, J. Non-Cryst. Solids **205-207**, 755 (1996).
[15] A. Gomez and S. A. Rice, J. Chem. Phys. **101**, 8094 (1994).
[16] M. Zhao, D. Chekmarev, Z. Cai, and S. A. Rice, Phys. Rev. E **56**, 7033 (1997).
[17] M. Zhao, D. Chekmarev, and S. A. Rice, J. Chem. Phys. **108**, 5055 (1998); M. Zhao and S. A. Rice, Internet J. Chem. **1**, URL: http://www.ijc.com/articles/1998v1/1/ (1998).
[18] O. M. Magnissen, B. M. Ocko, M. J. Regan, L. E. Berman, P. S. Pershan, and M. Deutsch, Phys. Rev. Lett. **74**, 4444 (1995).
[19] M. J. Regan, E. H. Kawamoto, S. Lee, P. S. Pershan, N. Maskil, M. Deutsch, O. M. Magnissen, B. M. Ocko, and L. E. Berman, Phys. Rev. Lett. **75**, 2498 (1995).
[20] M. J. Regan, O. M. Magnissen, E. H. Kawamoto, P. S. Pershan, B. M. Ocko, N. Maskil, M. Deutsch, S. Lee, K. Penanen, and L. E. Berman, J. Non-Cryst. Solids **205-207**, 762 (1996).
[21] M. J. Regan, H. C. Tostmann, P. S. Pershan, O. M. Magnussen, E. DiMasi, B. M. Ocko, and M. Deutsch, Phys. Rev. B **55**, 10 786 (1997).
[22] M. J. Regan, P. S. Pershan, O. M. Magnussen, B. M. Ocko, M. Deutsch, and L. E. Berman, Phys. Rev. B **54**, 9730 (1996).
[23] M. J. Regan, P. S. Pershan, O. M. Magnussen, B. M. Ocko, M. Deutsch, and L. E. Berman, Phys. Rev. B **55**, 15 874 (1997).
[24] B. N. Thomas, S. W. Barton, F. Novak, and S. A. Rice, J. Chem. Phys. **86**, 1036 (1987).
[25] E. B. Flom, M. Li, A. Acero, N. Maskil, and S. A. Rice, Science **260**, 332 (1993).
[26] E. B. Flom, Z. Cai, A. A. Acero, B. Lin, N. Maskil, L. Liu, and S. A. Rice, J. Chem. Phys. **96**, 4743 (1992).
[27] N. Lei, Z.-q. Huang, and S. A. Rice, J. Chem. Phys. **104**, 4802 (1996).
[28] N. Lei, Z.-q. Huang, S. A. Rice, and C. Grayce, J. Chem. Phys. **105**, 9615 (1996).
[29] N. Lei, Z.-q. Huang, and S. A. Rice, J. Chem. Phys. **107**, 4051 (1997).
[30] W. Kohn and L. J. Sham, Phys. Rev. **140**, A1133 (1965).
[31] A. G. Eguiluz, D. A. Campbell, A. A. Maradudin, and R. F. Wallis, Phys. Rev. B **30**, 5449 (1984).
[32] S. H. Vosko, L. Wilk, and M. Nusair, Can. J. Phys. **58**, 1200 (1980).
[33] D. C. Langreth and M. J. Mehl, Phys. Rev. B **28**, 1809 (1983).
[34] C. H. Woo, S. Wang, and M. Matsuura, J. Phys. F **5**, 1836 (1975).
[35] M. Matsuura, C. H. Woo, and S. Wang, J. Phys. F **5**, 1849 (1975).
[36] Y. Yaseda, *The Structure of Non-Crystalline Materials* (McGraw-Hill, New York, 1980).